

Supermassive Black Holes in Deep Multiwavelength Surveys

By C. MEGAN URRY¹ AND EZEQUIEL TREISTER²

¹Department of Physics, Yale University, P.O. Box 208121, New Haven, CT 06520-8121, USA

²European Southern Observatory, Casilla 19001, Santiago 19 Chile

In recent years deep X-ray and infrared surveys have provided an efficient way to find accreting supermassive black holes, otherwise known as active galactic nuclei (AGN), in the young universe. Such surveys can, unlike optical surveys, find AGN obscured by high column densities of gas and dust. In those cases, deep optical data show only the host galaxy, which can then be studied in greater detail than in unobscured AGN. Some years ago the hard spectrum of the X-ray “background” suggested that most AGN were obscured. Now GOODS, MUSYC, COSMOS and other surveys have confirmed this picture and given important quantitative constraints on AGN demographics. Specifically, we show that most AGN are obscured at all redshifts and the amount of obscuration depends on both luminosity and redshift, at least out to redshift $z \sim 2$, the epoch of substantial black holes and galaxy growth. Larger-area deep infrared and hard X-ray surveys will be needed to reach higher redshifts and to probe fully the co-evolution of galaxies and black holes.

1. Cosmic Growth of Black Holes and Galaxies

Abundant evidence indicates that the growth of a supermassive black hole is closely tied to the formation and evolution of the surrounding galaxy. The energy released from accretion onto the black hole affects star formation in the galaxy, probably limiting growth at the high- and low-mass ends, and of course the distribution and angular momentum of matter in the galaxy governs the amount of matter accumulated by the black hole (Silk & Rees 1998; King 2005; Rovilos *et al.* 2007). Emergent energy from accretion is also a factor in understanding ionization and radiation backgrounds (Hasinger 2000; Lawrence 2001). Understanding the growth history of these black holes is therefore critical to understanding the global evolution of structure in the Universe.

Yet the demographics of supermassive black holes remain elusive. The largest samples of quasars and Active Galactic Nuclei (AGN), by which we mean supermassive black holes in a high accretion-rate phase[†], have been found through optical selection (e.g., the Sloan Digital Sky Survey quasar sample; Schneider *et al.* 2002, 2007), but, at least locally, these are not representative of the larger AGN population. Instead we need surveys less biased against obscured AGN.

There are three reasons to suspect that most AGN are obscured by large column densities of gas and dust. First, a large body of evidence suggests that local AGN have geometries that are not spherically symmetric, and that different aspect angles present markedly different observed characteristics; this is referred to as AGN unification (Antonucci 1993; Urry & Padovani 1995). Second, AGN are more common at high redshift ($z \sim 2 - 3$), where the average star formation rate is higher and thus it is even more likely that gas and dust surround the galaxy nucleus than at $z \sim 0$. Third, and most important, obscured AGN are required to explain the shape of the X-ray “background” radiation.

The X-ray “background” is actually the superposition of individual AGN that were

[†] Some make a distinction between AGN and quasars, with the latter being above an arbitrary luminosity, typically $M_B = -23$ mag. Here we use the term AGN to refer to an actively accreting supermassive black hole above or below this luminosity.

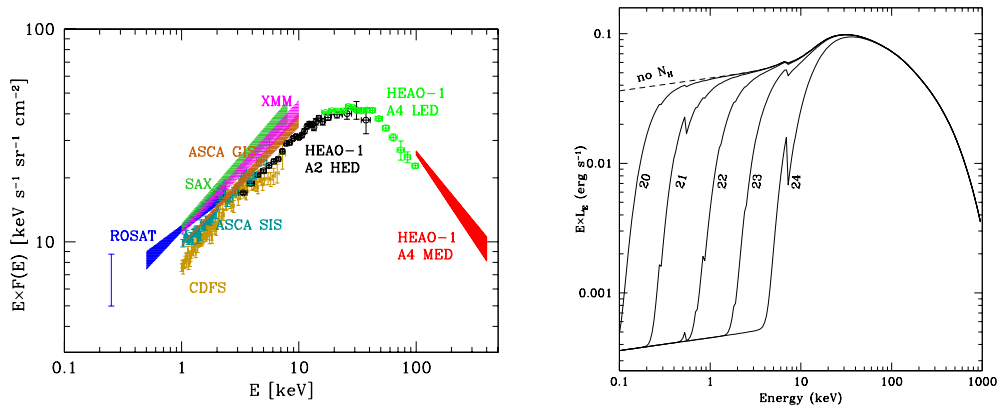


FIGURE 1. (*Left*) The X-ray background spectrum (shown in units of energy per logarithmic band) is very hard, peaking near 30 keV, in contrast to the spectra of unobscured AGN which are roughly horizontal in these units. (Figure from Gilli 2004.) (*Right*) Large column densities of gas absorb low-energy photons via the photoelectric effect, such that emission from an obscured AGN peaks at an energy that increases with column density. Each line represents a factor of 10 increase in equivalent N_H (lines are marked with $\log N_H$ in atoms/cm²; assumes solar abundances and the cross sections of Morrison & McCammon 1983).

not resolved in early X-ray experiments (hence the designation “background”). As shown in Figure 1a, its spectrum peaks at ~ 30 keV (i.e., this is where most of the energy is produced), much harder than the typical spectrum (roughly flat in these units) of an unobscured AGN. In obscured AGN, however, the softest X-ray photons have been absorbed via the photoelectric effect, and Compton-thick AGN (those with $N_H \geq 10^{24}$ cm⁻²) actually peak at roughly 30 keV (Fig. 1b). Thus X-ray observations have long indicated there is a large population of heavily obscured AGN (Setti & Woltjer 1989; Comastri *et al.* 1995; Gilli *et al.* 2001). While much of the X-ray background has been resolved at low energies, recent work on X-ray deep fields suggests the hardest (most obscured) X-ray sources have yet to be detected (e.g., Worsley *et al.* 2005).

Relatively unbiased AGN samples require joint hard X-ray and infrared surveys. Hard X-rays ($E > 2$ keV) penetrate all but the thickest column densities and efficiently locate black hole accretion. The absorbed optical through soft X-ray emission heats the surrounding dust and is re-radiated in the infrared, at wavelengths that depend on the dust temperature. Meanwhile, high-resolution optical surveys (e.g., with HST) allow separation of nuclear (AGN) and host galaxy light. Today, NASA’s three operating Great Observatories — the Chandra X-ray Observatory, the Spitzer Space Telescope, and the Hubble Space Telescope — enable matched X-ray, infrared, and optical surveys at unprecedented depth and resolution.

2. Deep Multiwavelength Surveys

The announcement in spring 2000 of the first Spitzer Legacy opportunity led to the Great Observatories Origins Deep Survey (GOODS), to date the deepest wide-area multiwavelength survey carried out with Spitzer, Hubble, and Chandra (Dickinson *et al.* 2003; Giavalisco *et al.* 2004). By targeting the Spitzer Legacy, and later the Hubble Treasury, observations on the pre-existing Chandra deep fields, we leveraged substantial investments of observing time, probed AGN demographics at the peak of quasar activity

($z \sim 1 - 2$), and enabled a wide range of other science, described in the *Astrophysical Journal Letters* special edition of January 10, 2004.†

The GOODS data are deep enough to detect AGN to very high redshift ($z \gtrsim 6$), and the volume sampled ensures sizable AGN samples out to $z \sim 3$. To sample larger volumes and to search effectively for rare objects like AGN or massive galaxies at high redshift, in 2002 we designed the MUSYC survey (Multiwavelength Survey by Yale and Chile), covering one square degree in two equatorial and two southern fields. Three of the four regions had already been observed extensively, including the Extended Chandra Deep Field South (ECDF-S) and the Extended Hubble Deep Field South (EHDF-S), thus leveraging substantial investments with Chandra, XMM-Newton, HST, and the largest ground-based telescopes.‡ Soon after starting MUSYC we helped start the COSMOS survey (Scoville *et al.* 2007b), a 2-square degree field centered at 1000+02 that has now been imaged extensively with HST, Spitzer, XMM, and Chandra.¶ The unprecedented combination of area and depth allow a wide variety of science, described in the September 2007 special edition of the *Astrophysical Journal Supplement*. Other relevant multiwavelength surveys include the Lockman Hole (Hasinger *et al.* 2001), CLASXS (Yang *et al.* 2004), the Extended Groth Strip (Davis *et al.* 2007), SWIRE (Lonsdale *et al.* 2003), XBOOTES (Hickox *et al.* 2006), HELLAS2XMM (Baldi *et al.* 2002), SEXSI (Harrison *et al.* 2003), CYDER (Treister *et al.* 2005), CHAMP (Kim *et al.* 2004), and AMSS (Akiyama *et al.* 2003).

3. Finding Obscured AGN

The question we set out to answer with GOODS, MUSYC, and COSMOS was, “Is there a substantial population of obscured AGN that is missed by traditional optical surveys?” To answer this question we need to sample the AGN population at $z \sim 1 - 2$, at the peak of the number density. The GOODS survey, and the Chandra Deep Field South (CDF-S) X-ray survey on which GOODS piggy-backed (Giacconi *et al.* 2002), were designed to sample the AGN population at $z \sim 0.5 - 2$, which includes the AGN that make up the X-ray background. Luminous AGN at higher redshifts could certainly be detected but the volume surveyed is too small to expect to see a reasonable number of them.

Early results in the CDFS and other deep X-ray fields showed there was a population of optically faint hard X-ray sources (Alexander *et al.* 2001; Franceschini *et al.* 2002b,a; Mainieri *et al.* 2005), which collectively comprised a large fraction of the integrated X-ray background intensity. However, as optical counterparts were identified and spectra obtained, several apparent problems emerged. First, the redshift distribution peaked at relatively low values, $z \lesssim 1$, lower than expected from the early population synthesis

† For more details see <http://www.stsci.edu/science/goods>.

‡ The four MUSYC fields include the ECDF-S, for which substantial additional Chandra observations were later acquired by N. Brandt (Lehmer *et al.* 2005; Virani *et al.* 2006); the EHD-F-S, for which there not yet any X-ray data; a field centered on a $z = 6.3$ quasar at 1030+05, which has relatively deep XMM data; and a new field centered at 1256+01 (“Castander’s Window”), an equatorial region with low 100-micron dust emission. The first two have now been imaged with Spitzer (IRAC and MIPS) and HST (ACS and NICMOS), and all fields are accessible with ALMA. For more details see <http://www.astro.yale.edu/MUSYC> and Gawiser *et al.* (2006b); Quadri *et al.* (2007); Gawiser *et al.* (2006a); van Dokkum *et al.* (2006).

¶ COSMOS is now one of the largest and best covered deep multiwavelength survey fields, representing the investment of thousands of hours of major telescope time (Scoville *et al.* 2007a; Sanders *et al.* 2007; Hasinger *et al.* 2007; Capak *et al.* 2007; Lilly *et al.* 2007). For more details, see <http://cosmos.astro.caltech.edu>.

models for the X-ray background. Second, the fraction of X-ray sources that were identified as obscured, either because of high N_H or absence of broad lines, was less than the canonical 3/4 seen at low redshift, and appeared to decline with redshift rather than increase, as specified by the best population synthesis model at that time (Gilli *et al.* 2001). A number of authors pointed out these problems (e.g., Mainieri *et al.* 2005; Rosati *et al.* 2002; Brandt & Hasinger 2005), and Franceschini *et al.* (2002*a*) suggested that “the unification scheme based on a simple orientation effect fails at high redshifts” and that the production of the X-ray background by a collection of obscured AGN “requires major revision.”

At the same time, these faint red X-ray AGN were copious emitters of infrared radiation (Treister *et al.* 2004, 2006), fully consistent with the unification paradigm. It also became apparent early on that, as for optically-selected quasars, the evolution of X-ray selected AGN is luminosity dependent, with high-luminosity AGN evolving earlier and more rapidly than low-luminosity AGN (Ueda *et al.* 2003; Cowie *et al.* 2003); this luminosity-dependent density evolution had not been incorporated in earlier population synthesis models for the X-ray background. Finally, we suspected that selection effects could play a significant role in affecting the redshifts and optical identifications of survey sources.

Accordingly, we developed a comprehensive quantitative approach, based on the unification scenario and incorporating the most recent, best luminosity function and evolution, to predict the number counts and redshift distributions at any wavelength (for the moment, infrared through X-ray, though it could be generalized) for surveys of arbitrary area, depth, and wavelength. Here we describe the quantitative interpretation of the multiwavelength data from GOODS, MUSYC, COSMOS and other deep multiwavelength surveys, including the dependence of the obscured fraction of AGN on luminosity and redshift. Specifically, we show that most AGN are obscured at all redshifts; that the fraction of obscured AGN decreases with luminosity; and that it increases with redshift, at least out to redshift $z \sim 2.5$, an epoch of substantial black hole and galaxy growth. Deep infrared and hard X-ray surveys over larger areas will be needed to reach higher redshifts and to probe fully the co-evolution of galaxies and black holes.

3.1. *Connecting X-Ray, Optical, and Infrared Surveys*

Our approach was to connect surveys at different wavelengths by assuming something sensible about AGN spectral energy distributions (SEDs), then combining those with well-measured luminosity functions and evolution to understand the source counts and redshift distributions of AGN selected at a given flux limit at any wavelength (Treister *et al.* 2004, 2006; Treister & Urry 2006; analogous approaches have been taken by Ballantyne *et al.* 2006 and Dwelly & Page 2006). Simultaneously, we constrain the same AGN population to fit the X-ray background (Treister & Urry 2005). An alternative approach is to model only the X-ray spectra of AGN and to fit the X-ray background alone with a mixture of obscured and unobscured AGN (Comastri *et al.* 1995; Gilli *et al.* 2001, 2007); this constrains the demographics but does not connect the X-ray sources to those detected at optical and infrared wavelengths — and thus does not use those additional constraints on the AGN demographics, nor does it allow a quantitative estimate of the important effect of optical or infrared flux limits on the survey content or spectroscopic identifications.

Briefly, our procedure was as follows: We started with the underlying AGN demographics, described by an AGN luminosity function that incorporates dependence on absorbing column density, and the luminosity-dependent evolution of this function (Ueda *et al.* 2003). Because this luminosity function is based on hard X-ray observations, it is relatively free of bias against obscured AGN.

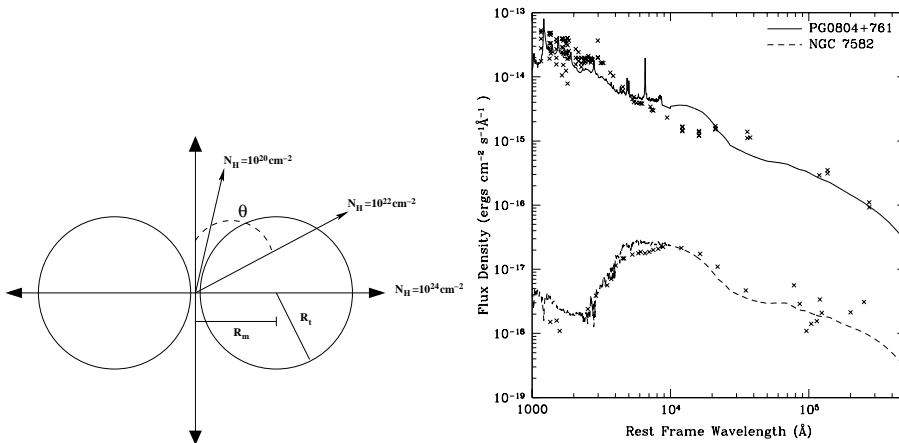


FIGURE 2. The infrared spectra of AGN were modeled by dust emission (Nenkova *et al.* 2002) from a clumpy torus geometry (*left*) that, assuming random orientations and adjusting the torus geometry to give a 3:1 ratio of column densities above:below $N_H = 10^{22} \text{ cm}^{-2}$, yields an N_H distribution consistent with various observational estimates (see text for details). (*Right*) Two examples of model SEDs (*lines*), which are fully determined from L_X and N_H . These fit very well the observed SEDs of local unobscured (*datapoints, top*) and obscured (*bottom*) AGN, with no free parameters. The composite model SEDs include infrared dust emission, reddened quasar spectra (keyed to N_H value), and an L_* host galaxy, linked to the X-rays by the known optical-to-X-ray ratio (which depends on L_X).

We then developed a set of SEDs, based on the unification paradigm, that represent AGN with a wide range in intrinsic luminosity and absorbing column density (parameterized in terms of the neutral hydrogen column density, N_H , along the line of sight). Specifically, at optical wavelengths ($\lambda=0.1\text{-}1$ microns), we used a Sloan Digital Sky Survey composite quasar spectrum (Vanden Berk *et al.* 2001) plus Milky-Way-type reddening laws and a standard dust-to-gas ratio to convert N_H to A_V ; we also added an L_* elliptical host galaxy, which is the dominant component for heavily obscured AGN. In the X-ray ($E > 0.5$ keV), we assumed a power-law spectrum with photon index $\Gamma = 1.9$, typical of unobscured AGN, absorbed by column densities in the range $\log N_H = 20\text{-}24 \text{ cm}^{-2}$. To describe the infrared part of the SEDs ($\lambda > 1$ micron), which in the unification paradigm includes radiation from dust heated by absorbed ultraviolet through soft X-ray photons, we used dust emission models by Nenkova *et al.* (2002) in a clumpy torus geometry (Fig. 2a), converting to N_H from viewing angle assuming random orientations. The resulting N_H distribution is completely consistent with various observational estimates (Ueda *et al.* 2003; Dwelly & Page 2006; Risaliti *et al.* 1999; Comastri *et al.* 1995; Tozzi *et al.* 2006; Gilli *et al.* 2007). AGN models with the same intrinsic X-ray luminosities were normalized at 100 microns. To connect the ultraviolet and X-ray parts of the SED we used the standard dependence of X-ray to optical luminosity ratio on luminosity (e.g., Steffen *et al.* 2006).

The SED models, parameterized in terms of L_X (as a proxy for intrinsic luminosity) and N_H (which depends only on viewing angle and torus geometry), describe extremely well the local population of AGN. There is some freedom in the choice of torus geometry, of course; we selected an aspect ratio that would produce three times as many AGN with N_H greater than 10^{22} cm^{-2} compared to smaller column densities (Fig. 2a), which is roughly the observed local ratio (Risaliti *et al.* 1999). Figure 2b shows the observed SEDs of two local AGN, one unobscured (top) and one heavily obscured (bottom), compared

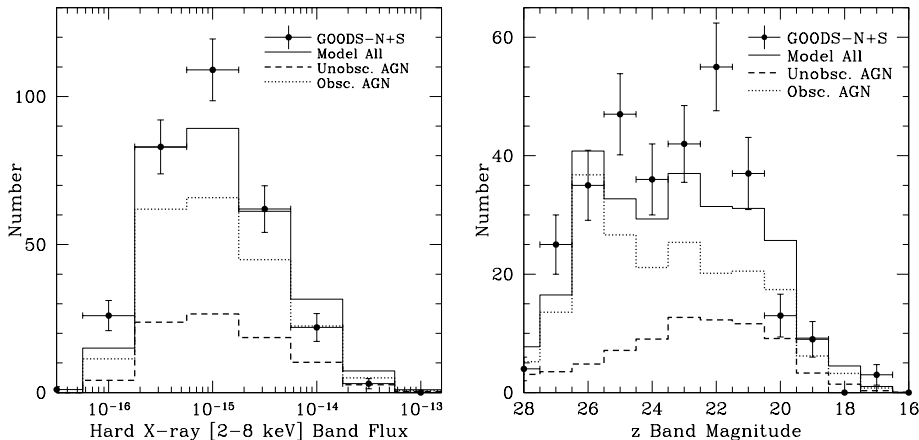


FIGURE 3. X-ray (*left*) and optical (*right*) counts observed in the GOODS fields (*data points*) agree well with a simple unification model (*solid line*), even with no dependence of torus geometry on luminosity or redshift (Treister *et al.* 2004). Inclusion of the luminosity dependence (found later in larger AGN samples) gives essentially the same result for the GOODS survey. Unobscured AGN ($N_H < 10^{22} \text{ cm}^{-2}$) dominate at bright optical magnitudes (*dashed line*) and obscured AGN ($N_H > 10^{22} \text{ cm}^{-2}$) at faint z-band magnitudes (*dotted line*). For $R > 24$ mag, the approximate limit for obtaining decent optical spectral identifications with 8-meter class telescopes, the vast majority of sources are obscured AGN.

to the model SED corresponding to the observed L_X and N_H . With no free parameters, the fit is remarkably good overall, meaning that this representation accurately reflects the distribution of photons across a very wide wavelength range.

Combining these model SEDs with the AGN luminosity function and evolution yields a distribution of sources as a function of spatial location and wavelength. For a given wavelength and flux limit, then, our calculation produces the expected number counts and redshift distribution of AGN. This population can be filtered by multiple flux limits (for example, one could look at the X-ray counts and redshift distribution of sources above arbitrary flux limits in the X-ray, optical, and infrared bands) and/or by other properties (e.g., N_H value). Our procedure was to generate the expected content of real surveys, and to compare to observations, in order to constrain the underlying AGN demographics, specifically, the AGN luminosity function, its evolution, its dependence on N_H , and the family of AGN SEDs (which includes the torus properties).

3.2. Quantitative Results from the Population Synthesis Model: Number Counts, Redshift Distributions, and the X-Ray Background

In a series of papers we showed that this straightforward model matches very well the observed properties of AGN samples. The first paper, Treister *et al.* (2004), assumed for the sake of simplicity that the torus geometry (and hence the N_H distribution) did not depend on luminosity or redshift. Even this simplest population synthesis model fits beautifully the observed X-ray and optical counts in the deep GOODS survey (Fig. 3). The source population at faint optical magnitudes, particularly the AGN too faint for identification with optical spectroscopy, is dominated by obscured AGN.

The unification-inspired model described above, like other population synthesis models (e.g., Gilli *et al.* 2001), predicts a large population of obscured AGN out to high redshift. The predicted peak of the redshift distribution (*dashed histogram*, Fig. 4a) is near $z \sim 1$, not much higher than that observed in the GOODS data (*shaded/open histogram*,

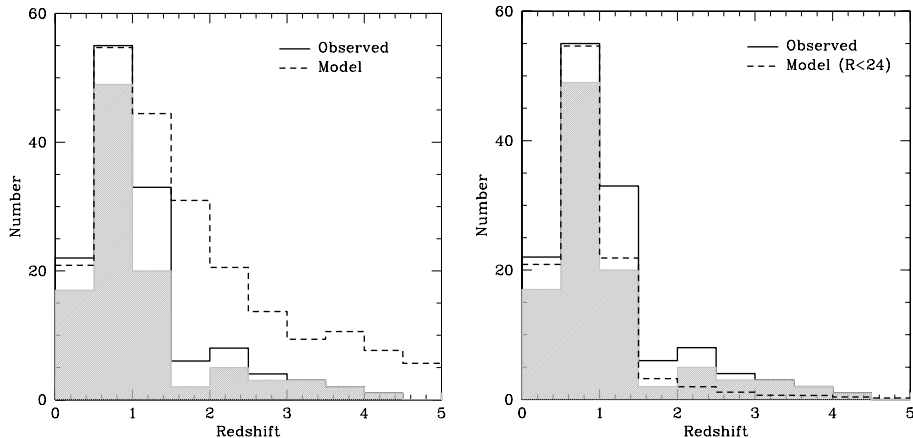


FIGURE 4. (Left) Observed spectroscopic redshift distribution (*hatched histogram*) and photometric redshift distribution (*open histogram*) for the GOODS-North field, compared to that expected from the unification model (*dashed line*). There is poor agreement at high redshifts. (Right) Imposing an optical flux limit on the model leads to an expected distribution (*dashed line*) that agrees very well with the observed distribution.

Fig. 4a), but there discrepancy at $z > 1$. Many of these high-redshift obscured AGN, because they are optically faint, are not identified in follow-up optical spectra of X-ray sources. This can be clearly seen imposing the spectroscopic limit, $R \sim 24$ mag, on the expected redshift distribution (*dashed histogram*, Fig. 4b); in this case, the observed and expected distributions agree well because the higher-redshift AGN remain largely unidentified. Equivalently, AGN without spectroscopic identifications will preferentially be faint, obscured sources.

The advent of multiple large AGN samples with high spectroscopic completeness allowed Barger *et al.* (2005) to deduce a dependence of obscured fraction on optical luminosity. We incorporated a simple functional form of that dependence in our model — namely, a linear transition between 100% of AGN with $L_X = 10^{42}$ ergs/s being obscured and no AGN with $L_X = 10^{46}$ ergs/s being obscured. Taking into account the selection effects due to flux limits, the model then matches the observed dependence very well (Fig. 11). The resulting number counts and redshift distributions for GOODS do not change, since only a restricted luminosity range (primarily 10^{43-44} ergs/s) is probed by that survey. In all work subsequent to Treister *et al.* (2004) — on infrared counts, X-ray background, and evolution of obscuration (see below) — we incorporated this luminosity dependence.

Our population synthesis model predicts, with very little freedom, the spectrum of the X-ray background. We simply sum the X-ray emission from all the AGN. There is some freedom in that we (like everyone else who does this kind of calculation) have to model the X-ray spectrum. We used an absorbed power law plus an iron line and a Compton-reflection hump, consistent with the AGN spectra that are well measured locally; we also assumed solar abundances and used the N_H distribution described above for $\log N_H = 20-24$ cm^{-2} . The N_H distribution for higher column densities ($N_H > 10^{24}$ cm^{-2}) is poorly constrained at present, so we extrapolated from $N_H < 10^{24}$ cm^{-2} with a flat slope (again, much like what others have assumed). Beyond this, one can adjust the metallicity (this increases the hard X-rays, holding everything else constant) or the include a small range of power-law slopes (ditto; Gilli *et al.* 2007), but we did not feel the data could constrain those parameters and so left them fixed. In any case, the integral constraint of the X-ray

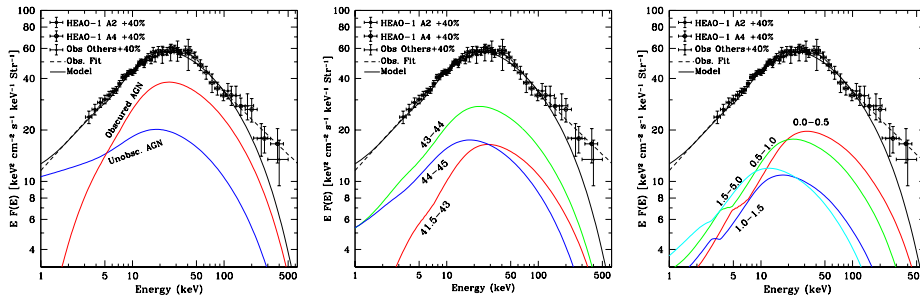


FIGURE 5. The predicted X-ray background spectrum (*heavy line*; Treister & Urry 2005) from the unification-inspired population synthesis model agrees very well with the observed data (*data points*). (*Left*) Obscured AGN (*thin, red, peaked curve*) dominate at high energies ($E > 10$ keV), while unobscured AGN (*thin, blue, broad curve*) dominate in the Chandra and XMM bands ($2 \text{ keV} < E < 10$ keV). There is little freedom in the fit parameters, especially at low energies, so this agreement is remarkably good. (Emission at $E > 100$ keV is dominated by blazars, which are not modeled here.) The X-ray background is dominated by moderate luminosity AGN, in the range 10^{43-44} ergs/s (*middle panel*) and by intermediate redshifts, $z \sim 0.5 - 1.5$ (*right panel*).

background is an excellent check on whether the demographics of AGN assumed here is realistic. Figure 5 shows that, with almost no free parameters, the data are very well fit indeed. (The normalization of the background at $E > 10$ keV is discussed below in § 3.3.)

Another strong prediction of the Treister model concerns the infrared data, which at the time the model was developed had not yet been taken. We calculated the expected Spitzer counts in IRAC and MIPS 24-micron bands; Figure 6 shows the excellent agreement with observations (Treister *et al.* 2006). Small discrepancies at the faint end are due to the overly simple assumption of a single host galaxy magnitude (which dominates at low fluxes), rather than a distribution.

From the Spitzer observations, we calculate the minimum AGN contribution to the extragalactic infrared background, obtaining a lower value than previously estimated, ranging from 2% to 10% in the 3-24 micron range (Treister *et al.* 2006). Accounting for heavily obscured AGN that, according to our population synthesis model, are not detected in X-rays, the AGN contribution to the infrared background increases by $\sim 45\%$, to $\sim 3-15\%$. Figure 7a shows the AGN contributions deduced from GOODS data (Treister *et al.* 2006) compared to other estimates and to the (uncertain) total extragalactic background light, as a function of infrared wavelength. The GOODS measurements place the strongest constraints to date on the AGN contribution to the extragalactic background light, indicating that stars dominate completely over AGN at infrared wavelengths.

The fraction of sources that are AGN rises sharply with $24 \mu\text{m}$ infrared flux (Fig. 7b). Thus in deep surveys like GOODS or COSMOS, AGN are a small fraction of the total infrared source population, while in high flux limit surveys like SWIRE (Lonsdale *et al.* 2003), they constitute a much higher fraction. AGN detected in large-area, shallow surveys are on average closer and/or more luminous than AGN found in deep pencil-beam surveys. We show in Figure 7b that this very strong dependence of AGN fraction on infrared flux is not an artifact of the X-ray flux limit. Specifically, using our AGN population synthesis model, we plot the number of AGN as a function of infrared flux including those too faint to be detected in X-rays in the Chandra Deep Fields (*open circles*). Clearly the trend is independent of X-ray flux limit.

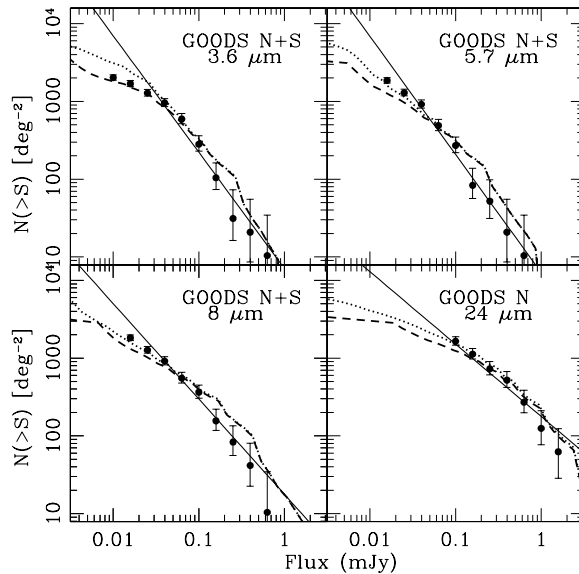


FIGURE 6. (*Filled circles*) Observed cumulative infrared flux distributions for X-ray detected AGN in the GOODS-North and South fields in three IRAC bands, and for the North field only in the MIPS 24-micron band. Error bars correspond to the 84% confidence level in the number of sources in that bin (Gehrels 1986). Because this is a cumulative plot, the bins are not independent. (*Solid line*) Power-law fit to the observed number counts. (*Dashed line*) Expected infrared flux distribution (Treister *et al.* 2006) based on our population synthesis model, taking into account the X-ray flux limit in the GOODS fields and the luminosity dependence of the obscured AGN fraction, and correcting for the effects of undersampling at the bright end caused by the small volume of the GOODS fields. (*Dotted line*) Expected infrared flux distribution not considering the X-ray flux limit (i.e., all sources expected from extrapolating the AGN luminosity function). In general, the model explains the normalization and shape of the counts quite well, especially considering the poor statistics at the bright end. At the faint end, where the host galaxy light dominates, the model diverges more significantly, since the model assumptions (no distribution in host galaxy magnitude or spectrum) are clearly far too simple.

3.3. Integral and Swift Hard X-Ray Surveys

If the population synthesis model presented here is correct, $\sim 50\%$ of AGN are currently missed even in deep X-ray surveys with *Chandra* or *XMM*. These are very obscured AGN, many of them Compton thick (i.e., $N_H > 10^{24} \text{ cm}^{-2}$), so all but the hardest X-ray surveys are biased against them. Fortunately, hard X-ray instruments on the INTEGRAL and Swift satellites can now reach fluxes below $\sim 10^{-11} \text{ ergs cm}^{-2} \text{ s}^{-1}$ at energies above 20 keV. Serendipitous AGN surveys at these energies covering almost the full sky have been carried out using Swift/BAT (Markwardt *et al.* 2005) and INTEGRAL/IBIS (Beckmann *et al.* 2006; Sazonov *et al.* 2007), yielding samples of ~ 100 AGN each. These surveys provide an unbiased view of the AGN population, independent of the amount of obscuration, although at present the sensitivity is sufficient to reach only local populations.

Figure 8a shows the logN-logS distribution from the INTEGRAL catalog (Sazonov *et al.* 2007) of AGN confirmed as Compton thick with N_H measurements from X-ray data. Clearly the original population synthesis model of Treister & Urry (2005) overpredicted the density of Compton-thick AGN by a factor of ~ 4 . This is not too surprising, as the model included assumptions that, at the time of the publication of that work, were

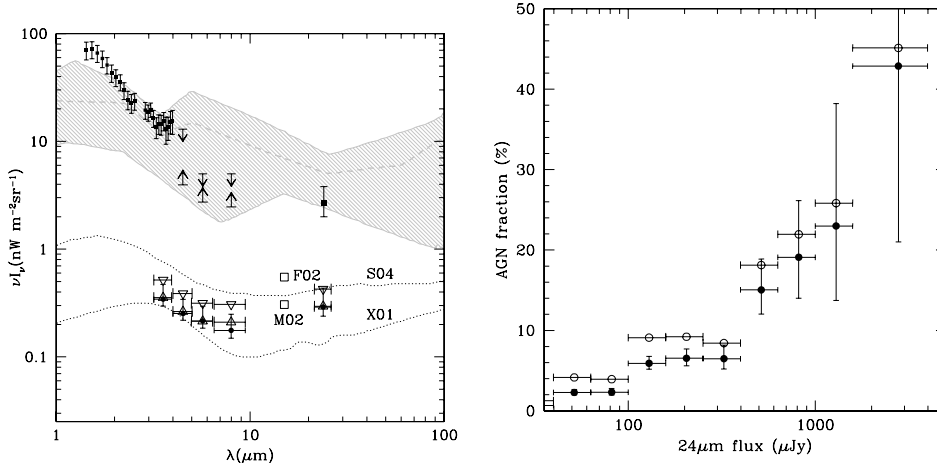


FIGURE 7. (*Left*) Extragalactic infrared background intensity as a function of wavelength. (*Shaded region*) Allowed values for the total intensity compiled by Hauser & Dwek (2001). 1-4 μm : Measurements reported by Matsumoto *et al.* (2005). 4-8 μm : Lower limits from Fazio *et al.* (2004), upper limits from Kashlinsky *et al.* (1996) at 4.5 μm and Stanev & Franceschini (1998) at 5.8 and 8 μm . Measurement at 24 μm from Papovich *et al.* (2004). (*Solid circles*) Integrated infrared emission from X-ray-detected AGN in the GOODS fields, with 1σ error bars from source number statistics (which dominate over measured flux errors) calculated as in Gehrels (1986). (*Triangles*) Integrated AGN emission from the models of Treister & Urry (2005) if only X-ray-detected AGN are considered (*lower*) or including all AGN (*upper*). (*Dotted lines*) Expected AGN integrated emission from the AGN models of Silva *et al.* (2004; *upper line*) and Xu *et al.* (2001; *lower line*). (*Open squares*) Expected AGN integrated emission at 15 μm from the extrapolation to fainter fluxes of IRAS and ISO (Matute *et al.* 2002 [M02]; corrected by a factor of 5 to include the contribution from obscured AGN) and ISO only (Fadda *et al.* 2002 [F02]) observations. (*Right*) The fraction of sources that are AGN rises sharply with 24 μm infrared flux (*filled circles*). Vertical error bars show the 1σ Poissonian errors on the number of sources (Gehrels 1986). Also shown is the contribution corrected by the AGN expected to be missed by X-ray selection (*open circles*), as estimated using our AGN population synthesis model; this shows the same strong dependence on infrared flux, indicating that that dependence is not a selection effect induced by the X-ray flux limit.

unconstrained — for example, the reflection fraction[†] was assumed to be unity, and the number of Compton-thick AGN was simply extrapolated with a flat slope from the N_H distribution at lower column densities.

Now we explore the constraints on these quantities that come from the new Swift and INTEGRAL surveys. First, we define a “Compton-thick AGN correction factor,” which simply multiplies the original flat-extrapolation assumption to match the observed number density of AGN with $N_H > 10^{24} \text{ cm}^{-2}$. According to a χ^2 minimization, the best-fit value for the Compton-thick AGN factor is 0.25; this produces a good agreement between model and observations, with a reduced χ^2 of 0.3.

Second, we consider the ratio of direct and reflected X-rays. The spectrum of Compton-thick AGN at high energies is dominated by the Compton reflection component (e.g., Matt *et al.* 2000), which has a strong peak at $E \sim 30 \text{ keV}$ (Magdziarz & Zdziarski 1995). The observed spectrum of the X-ray background, which we now understand as the integrated emission from previously unresolved AGN, also has peak at about the same energy (Gruber *et al.* 1999). The normalization of the reflection component relative to the direct

[†] The reflection fraction is the geometrical factor describing the solid angle, relative to 2π , subtended by cold reflecting material as seen from the primary X-ray source.

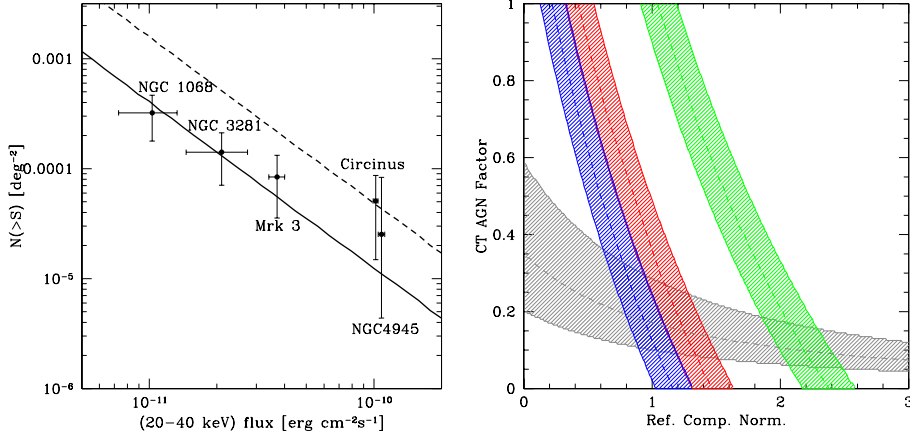


FIGURE 8. (*Left*) LogN-logS relation for Compton-thick AGN only. The *dashed line* shows the original prediction of Treister & Urry (2005), which assumed a reflection component normalization of 1 and a Compton-thick AGN factor of 1 (i.e., as many Compton-thick AGN as Compton-thin AGN in the next lowest decade of the N_H distribution). Data points are from the INTEGRAL survey of Sazonov *et al.* (2007). The population synthesis model can be brought to agreement with the observations if there are a factor of 4 fewer Compton-thick AGN (i.e., the Compton-thick AGN factor is 0.25). (*Right*) Compton-thick AGN factor versus normalization of the Compton reflection component. The *gray region* shows the values of these parameters that produce a space density of Compton-thick AGN consistent with the observed value in the Sazonov *et al.* (2007) sample, considering $1-\sigma$ statistical fluctuations. The allowed values of the parameters needed to fit the intensity of the X-ray background at 20-40 keV, assuming a 5% uncertainty in each case, are shown by the *blue region* for the original Gruber *et al.* (1999) measurements, the *red region* for the INTEGRAL values and by the *green region* for the Gruber *et al.* (1999) points increased by 40% (which was the assumption in Treister & Urry 2005). A large value of the reflection component is required to obtain values consistent with the latter X-ray background intensity, inconsistent with observations of the reflection component in individual AGN. Both the reflection value and the renormalization of the Gruber *et al.* (1999) X-ray background intensity must be lower.

emission is known only for a few nearby AGN, mostly from BeppoSAX observations (e.g., Perola *et al.* 2002), and therefore this parameter is usually taken as an assumption in AGN population synthesis models that can explain the spectral shape and intensity of the X-ray background. The resulting peak X-ray background intensity depends on both the assumed space density of Compton-thick AGN and the normalization of the reflection component, R ; while satisfying the overall intensity constraint, one can trade increased reflection for fewer Compton-thick AGN, or vice versa. Figure 8b shows the allowed regions in terms of the Compton-thick AGN factor versus reflection parameter. That is, the shaded regions show the values of these two parameters that produce an integrated X-ray background intensity in the 20-40 keV range, the region most affected by both the number of Compton-thick AGN and R , consistent with: (*green region*) the Gruber *et al.* (1999) data increased by 40% (the maximum suggested renormalization to match higher estimates with imaging instruments at lower energies; Treister & Urry 2005); (*red region*) the recent INTEGRAL X-ray background intensity measured using Earth occultation by Churazov *et al.* (2006); (*blue region*) the original Gruber *et al.* (1999) measurements, not renormalized. In each case uncertainties in the X-ray background intensity were assumed to be 5%. The gray shaded region shows the parameter space that produces a density of Compton-thick AGN consistent with the observations in Fig. 8a.

Previously, Treister & Urry (2005) assumed an X-ray background intensity consistent

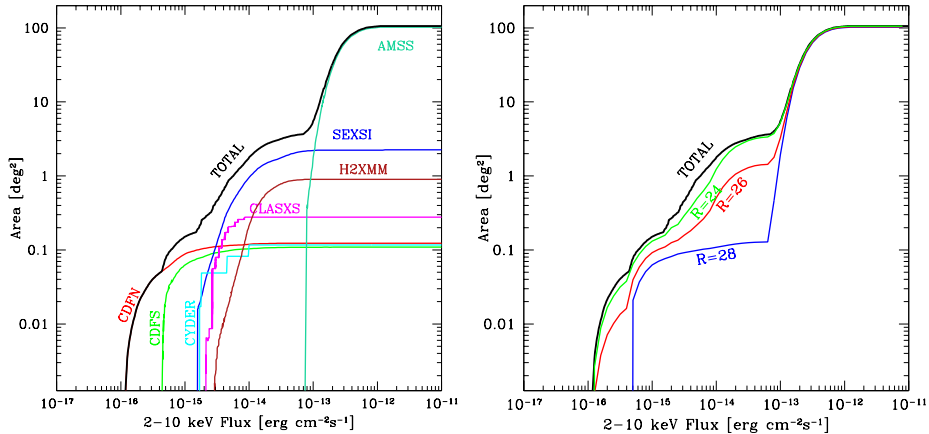


FIGURE 9. (*Left*) Area versus hard X-ray flux for each of the seven surveys combined in this work (*light colored lines*) and for the total sample (*thick black line*). (*Right*) Total effective area as a function of X-ray flux and optical magnitude (for $R=24$, 26 and 28 mag), taking into account the spectroscopic incompleteness of each survey (see text for details). These curves are used to compute the expected fraction of identified obscured AGN for an intrinsically non-evolving ratio.

with the Gruber *et al.* (1999) value increased by 40%, which was well fit by a Compton-thick AGN factor of 1 (flat extrapolation of the N_H distribution; Fig. 5). However, such a high value of the Compton-thick AGN factor is clearly inconsistent with the new observational constraints on the density of Compton-thick AGN. So, either the intensity of the X-ray background is lower, as suggested by recent INTEGRAL measurements (Churazov *et al.* 2006), or the average value of the reflection parameter is high, $R \sim 2$, or some combination of the two. Observations of individual sources seem to indicate that such a high value for the reflection component is unlikely. From a sample of 22 Seyfert galaxies, excluding Compton-thick sources, Malizia *et al.* (2003) concluded that both obscured and unobscured sources have similar reflections component with normalization values in the 0.6-1 range. A similar value of $R \simeq 1$ was reported by Perola *et al.* (2002) based on BeppoSAX observations of a sample of nine Seyfert 1 galaxies. Although with large scatter, normalizations for the average reflection component of 0.9 for Seyfert 1 and 1.5 for Seyfert 2 were measured from BeppoSAX observations of a sample of 36 sources (Deluit & Courvoisier 2003). Therefore, a value of $R \sim 1$ for the normalization of the reflection component, required by both the observed Compton-thick AGN space density and the X-ray background intensity reported by INTEGRAL and HEAO-1, is in good agreement with the observed values in nearby Seyfert galaxies.

4. Evolution of the Obscured Fraction of AGN

The X-ray background, being an integral constraint, is not a strong probe of the fraction of AGN that is obscured (as we showed in the previous section), much less of the evolution of that fraction with cosmic epoch. As shown in Figure 5, a simple population synthesis model in which obscured and unobscured AGN have the same evolution (or equivalently, the fraction of AGN that is obscured does not evolve) is fully consistent with the spectrum of the X-ray background. Now, however, the large X-ray samples that have become available in the past few years, spanning a range of depths and with

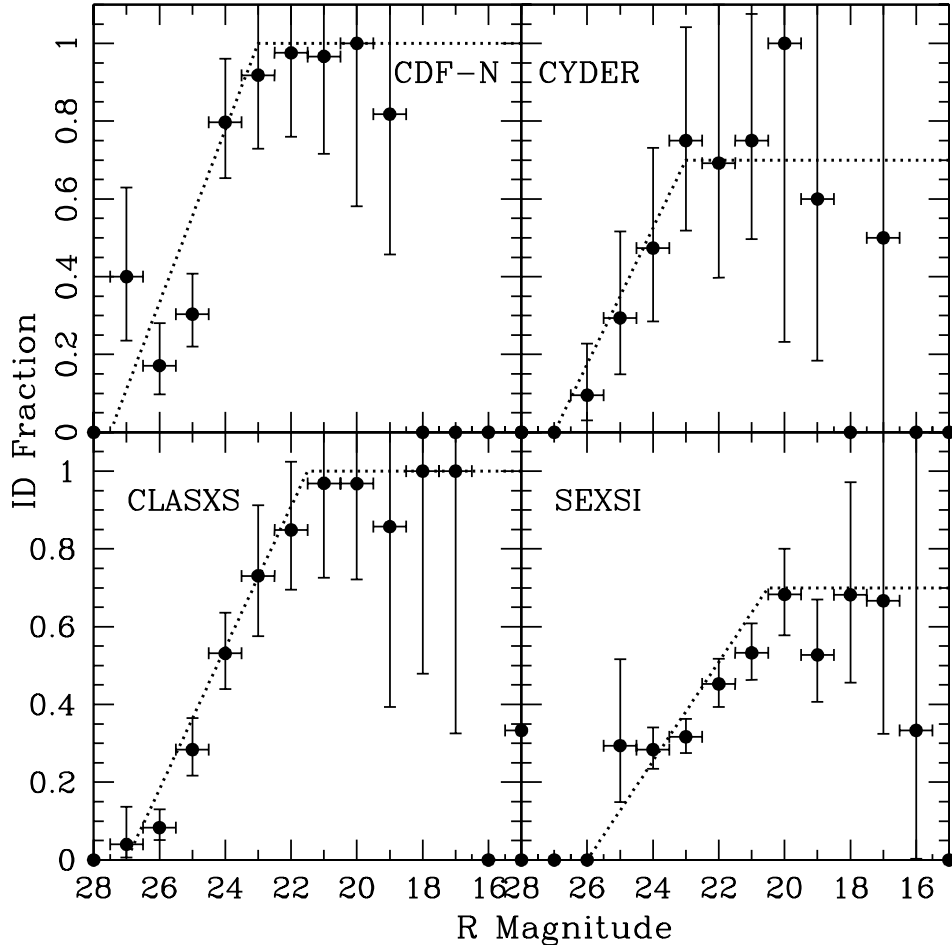


FIGURE 10. Fraction of optically identified AGN as a function of optical magnitude (*data points*), for four of the seven surveys comprising our super-sample. All seven are well described by a simple linear increase to a constant fraction at bright magnitudes (*lines*). This allows us to derive the effective survey area as a function of both X-ray flux and optical magnitude.

high spectroscopic completeness, allow us to determine whether and how the fraction of obscured AGN depends on redshift (Treister & Urry 2006).

To study the evolution of the obscured AGN fraction, one needs to distinguish between the effects of redshift and luminosity, which are correlated in any flux-limited sample. Wide area, shallow X-ray surveys (e.g., XBOOTES; Hickox *et al.* 2006) sample moderate luminosity AGN at low redshifts and only high luminosity sources up to high redshifts, while deep pencil-beam surveys (e.g., CDFS; Giacconi *et al.* 2002) find moderate luminosity AGN out to high redshifts but lack rare, high-luminosity sources because of the small volume sampled. Combining the two extremes covers the luminosity-redshift plane effectively.

We generate an AGN super-sample comprising seven large surveys with high identification fractions: AMSS (Akiyama *et al.* 2003), SEXSI (Harrison *et al.* 2003), HEL-LAS2XMM (Baldi *et al.* 2002), CLASXS (Yang *et al.* 2004), CYDER (Treister *et al.*

2005), and the two Chandra deep fields (Giacconi *et al.* 2002; Alexander *et al.* 2003). This super-sample contains a total of 2341 hard X-ray-selected AGN (X-ray sources with $L_X > 10^{42}$ ergs/s), the largest such sample to date by a factor of ~ 4 (Treister & Urry 2006). It spans a range of luminosities at each redshift, over a broad redshift range. The total area of this super-sample as a function of X-ray flux is shown in Figure 9a.

More than half the super-sample is optically identified. We define an AGN as unobscured when there is evidence for broad emission lines in their spectra, and as obscured AGN otherwise. The “obscured fraction” is then the number of obscured AGN divided by the total number of AGN. For obvious reasons, the identified fraction of any survey depends on the brightness of the optical counterparts. We parameterized the identified fraction of each of the seven surveys with a simple function that is constant at bright magnitudes and falls linearly to faint magnitudes (Fig. 10; see Treister & Urry 2006 for details). We then weight the area versus X-ray flux curve (Fig. 9a) by the completeness at each optical magnitude, for each survey, and sum those to get the effective area of the super-sample as a function of both X-ray flux and optical magnitude (Fig. 9b). This allows us to calculate the expected numbers of optically identified AGN for the super-sample, i.e., we can now correct for both X-ray and optical spectroscopic limits.

As discussed earlier (§ 3.2), the fraction of obscured AGN depends on luminosity (Barger *et al.* 2005). Our population synthesis model assumed a linear transition between 100% obscured fraction at $L_X = 10^{42}$ ergs/s and 0 obscured fraction at $L_X = 10^{46}$ ergs/s. Taking into account the selection effects due to flux limits (Fig. 9b), this assumption (*black line*, Fig. 11) matches the observed dependence very well in the present super-sample (*black line*, Fig. 11). The somewhat shallower luminosity dependence adopted by (Gilli *et al.* 2007; *blue dashed line* is their assumed dependence, *red dotted line* incorporates flux limits), in contrast, does not describe the obscured fraction well for high-luminosity AGN, probably because their model was constrained by the X-ray background, which is dominated by moderate luminosity AGN.

Our population synthesis model fits the X-ray, optical, and infrared counts of AGN; the X-ray background (modulo the trade-off between the number of Compton-thick AGN and the reflection fraction of each); the hard X-ray counts measured with Swift and INTEGRAL (ditto); and the observed luminosity dependence of the obscured fraction of AGN in the largest AGN sample to date. What can it tell us about the evolution of this obscured fraction?

Figure 12a shows the observed fraction as a function of redshift (*black data points*). As many have noted previously, the observed fraction declines with redshift, from roughly 3/4 locally to $\sim 1/3$ at $z \sim 4$. This has been interpreted to mean that obscured AGN are rare at high redshift. However, the lines in Figure 12a show the expected decline for an underlying population whose obscured fraction is actually constant with redshift, calculated for our super-sample using the appropriate corrections for X-ray and optical flux limits and spectroscopic completeness. That is, an even steeper decline is expected in the observed samples even when the underlying population does not change at all with redshift.

Three significant selection effects cause this strong decline. First, obscured AGN have smaller X-ray fluxes, so there is a bias against their detection in the X-ray sample in the first place. This is a small effect, particularly because it becomes relatively less important with increasing redshift (for which rest-frame emission is in an increasingly harder X-ray band affected only by higher and higher column densities). Second, obscured AGN are fainter in the optical, so there is a bias against spectroscopic identifications for $z \gtrsim 1$ (Treister *et al.* 2004); this is not important for samples with highly complete spectroscopic identifications. Third and quite important, the obscured fraction depends

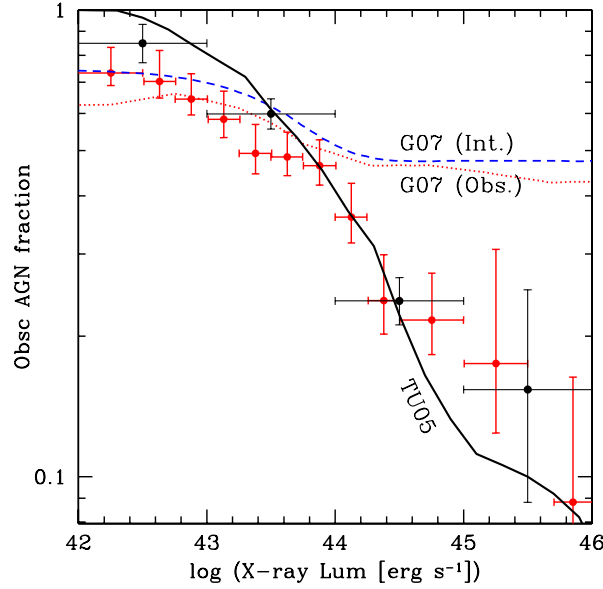


FIGURE 11. Fraction of obscured AGN in the super-sample as a function of hard X-ray luminosity. (*Black data points*) Observed distribution for the super-sample described in this work. (*Red data points*) Compilation of G. Hasinger (2007, in prep.) used in the work reported by Gilli *et al.* (2007). (*Black solid line*) Expected luminosity dependence for the Treister population synthesis models, taking into account the X-ray flux limit and spectroscopic completeness of the super-sample described here (Treister & Urry 2006). (*Blue dashed and red dotted lines*) Intrinsic and bias-corrected (i.e., expected) luminosity dependences for the population synthesis model of Gilli *et al.* (2007). This assumed luminosity dependence is not a good description of AGN demographics at higher luminosities; the Gilli *et al.* 2007 model is constrained primarily by the X-ray background intensity, which is dominated by moderate luminosity AGN.

strongly on luminosity (Fig. 11). Given the luminosity-redshift correlation inherent in flux-limited samples, the mean AGN luminosity increases with redshift and therefore the obscured fraction that is observed decreases — even if the same population of obscured lower-luminosity AGN is present. Our analysis shows that this is the dominant selection effect. It is an important effect even in AGN samples with 100% complete spectroscopic identifications, as indicated by the blue line in Figure 12a. Simply put, high redshift AGN samples are biased to higher luminosity, and thus contain lower obscured fractions, even if there is no underlying evolution of the ratio between obscured and unobscured AGN at all.

The observed more gradual decline in obscured fraction of AGN actually implies an increase in obscured fraction with redshift. Figure 12b shows the data relative to (i.e., divided by) the expectation for a non-evolving population, for the super-sample and the two sub-samples with higher identification fractions. The effect is largely independent of the completeness of the optical identifications. Fitting the increasing fraction with a simple power-law dependence on redshift, $\propto (1+z)^\alpha$, gives a good fit for $\alpha = 0.4 \pm 0.1$. This means that the fraction of AGN at redshift $z \sim 4$ that are obscured is observed to be twice as high as would be the case were the intrinsic fraction constant. AGN obscuration is substantially greater in the young Universe.

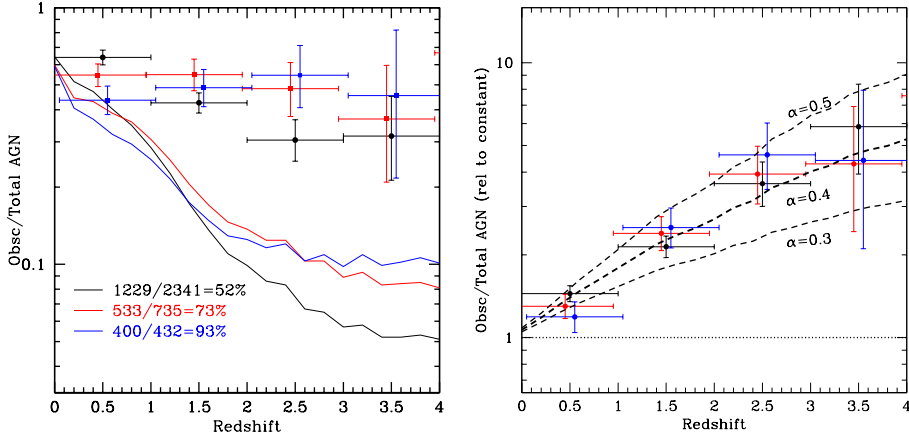


FIGURE 12. (*Left*) Observed fraction of obscured AGN as a function of redshift. (*Data points*) Measured fraction for our super-sample of 1229 optically-classified AGN (*black points*), and for sub-samples cut at brighter optical magnitudes to increase the spectroscopic completeness to 73% (*red points*) and 93% (*blue points*). (*Solid lines*) Expected fraction as a function of redshift for an intrinsically non-evolving ratio, taking into account the effects of spectroscopic incompleteness and flux limits for the super-sample and two sub-samples. (*Right*) Fraction of obscured AGN relative to the expectations for a non-evolving obscured AGN ratio (*dotted line*), incorporating the effects of spectroscopic incompleteness. A significant increase with redshift is clearly seen, independent of the spectroscopic completeness of the sample. *Dashed lines* show an intrinsic evolution of the form $(1+z)^\alpha$, for $\alpha = 0.4 \pm 0.1$.

5. Summary

GOODS, MUSYC, and other deep multiwavelength surveys provide overwhelming evidence for a large population of obscured AGN that dominate AGN demographics out to high redshifts. Optical surveys are biased against detecting these objects, and even hard X-ray surveys, which are considerably less biased, suffer strong selection effects, primarily due to the luminosity-dependence of obscuration.

Taking these effects into account quantitatively, with a realistic, well-constrained population synthesis model that uses AGN spectral energy distributions based on a unification paradigm, we deduce that the ratio of obscured ($N_H > 10^{22} \text{ cm}^{-2}$) to unobscured ($N_H < 10^{22} \text{ cm}^{-2}$) AGN is roughly 3:1 locally (integrated over all luminosities), and increases with redshift. Low-luminosity AGN ($10^{42} \text{ ergs/s} < L_X < 10^{44} \text{ ergs/s}$) are much more likely to be obscured than high-luminosity AGN ($L_X > 10^{44} \text{ ergs/s}$).

To the extent that our assumed infrared through X-ray spectral energy distributions are reasonable, and our assumed N_H distribution is reasonable (it is essentially the same as that used by others in the field; see Gilli *et al.* 2007 for a comparison of the different distributions), these results are completely robust.

How might one avoid the biases inherent in optical and X-ray surveys? In principle, far-infrared surveys are unbiased because the absorbed energy is re-radiated thermally; however, infrared surveys are very inefficient for AGN selection since the infrared sky is strongly dominated by starlight (Fig. 7a). In addition, AGN signatures (such as broad emission lines, strong power-law continua, and rapid variability) may well be hidden in obscured objects. Thus, identifying complete samples of AGN from far-infrared surveys will never be a simple matter, although it can potentially put useful limits on the fraction of galaxies with buried AGN.

Selection effects are very important to take into account for any survey, even those

that are 100% identified. For example, consider a deep hard X-ray survey for which all sources have optical and/or infrared counterparts with known redshifts and classification. Many would assume the survey itself is not strongly biased and that the identifications yield the underlying demographics, since no X-ray sources remain unidentified. However, missing from the X-ray sample are the most heavily obscured AGN; even more important, unobscured AGN are over-represented (relative to their fraction of the underlying population), especially at high redshift, because of the dependence of obscuration on luminosity. This in fact is the dominant effect for existing surveys.

Therefore, to understand the distribution of black holes in the universe and to estimate cosmic accretion rates, the selection effects must be modeled using reasonable assumptions about the underlying population. That in turn yields a picture of the universe that matches well our picture of nascent accreting black holes at the centers of dusty, star-forming, young galaxies in the early Universe.

This work would not have been possible without the exquisite data made possible by NASA's Great Observatories and by great observatories on the ground. We gratefully acknowledge support from NSF grant AST-0407295 and NASA grants NAG5-10301, HST-AR-10689.01-A, HST-GO-09822.09-A, HST-GO-09425.13-A, and NNG05GM79G.

REFERENCES

- AKIYAMA, M., UEDA, Y., OHTA, K., TAKAHASHI, T. & YAMADA, T. 2003 Optical Identification of the ASCA Medium Sensitivity Survey in the Northern Sky: Nature of Hard X-Ray-Selected Luminous Active Galactic Nuclei. *ApJ* **148**, 275–315.
- ALEXANDER, D. M., BAUER, F. E., BRANDT, W. N., SCHNEIDER, D. P., HORNSCHEMEIER, A. E., VIGNALI, C., BARGER, A. J., BROOS, P. S., COWIE, L. L., GARMIRE, G. P., TOWNSLEY, L. K., BAUTZ, M. W., CHARTAS, G. & SARGENT, W. L. W. 2003 The Chandra Deep Field North Survey. XIII. 2 Ms Point-Source Catalogs. *AJ* **126**, 539–574.
- ALEXANDER, D. M., BRANDT, W. N., HORNSCHEMEIER, A. E., GARMIRE, G. P., SCHNEIDER, D. P., BAUER, F. E. & GRIFFITHS, R. E. 2001 The Chandra Deep Field North Survey. VI. The Nature of the Optically Faint X-Ray Source Population. *AJ* **122**, 2156–2176.
- ANTONUCCI, R. 1993 Unified models for active galactic nuclei and quasars. *ARA&A* **31**, 473–521.
- BALDI, A., MOLENDI, S., COMASTRI, A., FIORE, F., MATT, G. & VIGNALI, C. 2002 The HELLAS2XMM Survey. I. The X-Ray Data and the logN-logS Relation. *ApJ* **564**, 190–195.
- BALLANTYNE, D. R., EVERETT, J. E. & MURRAY, N. 2006 Connecting Galaxy Evolution, Star Formation, and the Cosmic X-Ray Background. *ApJ* **639**, 740–752.
- BARGER, A. J., COWIE, L. L., MUSHOTZKY, R. F., YANG, Y., WANG, W.-H., STEFFEN, A. T. & CAPAK, P. 2005 The Cosmic Evolution of Hard X-Ray-selected Active Galactic Nuclei. *AJ* **129**, 578–609.
- BECKMANN, V., GEHRELS, N., SHRADER, C. R. & SOLDI, S. 2006 The First INTEGRAL AGN Catalog. *ApJ* **638**, 642–652.
- BRANDT, W. N. & HASINGER, G. 2005 Deep Extragalactic X-Ray Surveys. *ARA&A* **43**, 827–859.
- CAPAK, P., AUSSEL, H., AJIKI, M., MCCracken, H. J., MOBASHER, B., SCOVILLE, N., SHOP-BELL, P., TANIGUCHI, Y., THOMPSON, D., TRIBIANO, S., SASAKI, S., BLAIN, A. W., BRUSA, M., CARILLI, C., COMASTRI, A., CAROLLO, C. M., CASSATA, P., COLBERT, J., ELLIS, R. S., ELVIS, M., GIAVALISCO, M., GREEN, W., GUZZO, L., HASINGER, G., ILBERT, O., IMPEY, C., JAHNKE, K., KARTALTEPE, J., KNEIB, J.-P., KODA, J., KOEKE-MOER, A., KOMIYAMA, Y., LEAUTHAUD, A., LEFEVRE, O., LILLY, S., LIU, C., MASSEY, R., MIYAZAKI, S., MURAYAMA, T., NAGAO, T., PEACOCK, J. A., PICKLES, A., PORCIANI, C., RENZINI, A., RHODES, J., RICH, M., SALVATO, M., SANDERS, D. B., SCARLATA, C., SCHIMINOVICH, D., SCHINNERER, E., SCODEGGIO, M., SHETH, K., SHIOYA, Y., TASCIA,

- L. A. M., TAYLOR, J. E., YAN, L. & ZAMORANI, G. 2007 The First Release COSMOS Optical and Near-IR Data and Catalog. *ApJ* **172**, 99–116.
- CHURAZOV, E., SUNYAEV, R., REVNIVTSEV, M., SAZONOV, S., MOLKOV, S., GREBENEV, S., WINKLER, C., PARMAR, A., BAZZANO, A., FALANGA, M., GROS, A., LEBRUN, F., NATALUCCI, L., UBERTINI, P., ROQUES, J. ., BOUCHET, L., JOURDAIN, E., KNOEDLSEDER, J., DIEHL, R., BUDTZ-JORGENSEN, C., BRANDT, S., LUND, N., WESTERGAARD, N. J., NERONOV, A., TURLER, M., CHERNYAKOVA, M., WALTER, R., PRODUIT, N., MOWLAVI, N., MAS-HESSE, J. M., DOMINGO, A., GEHRELS, N., KUULKERS, E., KRETSCHMAR, P. & SCHMIDT, M. 2006 INTEGRAL observations of the cosmic X-ray background in the 5-100 keV range via occultation by the Earth. *ArXiv Astrophysics e-prints* .
- COMASTRI, A., SETTI, G., ZAMORANI, G. & HASINGER, G. 1995 The contribution of AGNs to the X-ray background. *A&A* **296**, 1–4.
- COWIE, L. L., BARGER, A. J., BAUTZ, M. W., BRANDT, W. N. & GARMIRE, G. P. 2003 The Redshift Evolution of the 2-8 keV X-Ray Luminosity Function. *ApJ* **584**, L57–L60.
- DAVIS, M. *et al.* 2007 The All-Wavelength Extended Groth Strip International Survey (AEGIS) Data Sets. *ApJ* **660**, L1–L6.
- DELUIT, S. & COURVOISIER, T. J.-L. 2003 The intrinsic emission of Seyfert galaxies observed with BeppoSAX/PDS. I. Comparison of the average spectra of the three classes of Seyfert galaxies. *A&A* **399**, 77–90.
- DICKINSON, M., GIAVALISCO, M. & THE GOODS TEAM 2003 The Great Observatories Origins Deep Survey. In *The Mass of Galaxies at Low and High Redshift* (ed. R. Bender & A. Renzini), pp. 324–+.
- DWELLY, T. & PAGE, M. J. 2006 The distribution of absorption in AGN detected in the XMM-Newton observations of the CDFS. *MNRAS* **372**, 1755–1775.
- FADDA, D., FLORES, H., HASINGER, G., FRANCESCHINI, A., ALTIERI, B., CESARSKY, C. J., ELBAZ, D. & FERRANDO, P. 2002 The AGN contribution to mid-infrared surveys. X-ray counterparts of the mid-IR sources in the Lockman Hole and HDF-N. *A&A* **383**, 838–853.
- FAZIO, G. G., ASHBY, M. L. N., BARMBY, P., HORA, J. L., HUANG, J.-S., PAHRE, M. A., WANG, Z., WILLNER, S. P., ARENDT, R. G., MOSELEY, S. H., BRODWIN, M., EISENHARDT, P., STERN, D., TOLLESTRUP, E. V. & WRIGHT, E. L. 2004 Number Counts at $3 \mu\text{m} < \lambda < 10 \mu\text{m}$ from the Spitzer Space Telescope. *ApJ* **154**, 39–43.
- FRANCESCHINI, A., BRAITO, V. & FADDA, D. 2002*a* Origin of the X-ray background and AGN unification: new perspectives. *MNRAS* **335**, L51–L56.
- FRANCESCHINI, A., FADDA, D., CESARSKY, C. J., ELBAZ, D., FLORES, H. & GRANATO, G. L. 2002*b* Infrared Space Observatory Investigates the Nature of Extremely Red Hard X-Ray Sources Responsible for the X-Ray Background. *ApJ* **568**, 470–474.
- GAWISER, E., VAN DOKKUM, P. G., GRONWALL, C., CIARDULLO, R., BLANC, G. A., CASTANDER, F. J., FELDMEIER, J., FRANCKE, H., FRANX, M., HABERZETTL, L., HERRERA, D., HICKEY, T., INFANTE, L., LIRA, P., MAZA, J., QUADRI, R., RICHARDSON, A., SCHAWINSKI, K., SCHIRMER, M., TAYLOR, E. N., TREISTER, E., URRY, C. M. & VIRANI, S. N. 2006*a* The Physical Nature of Ly α -emitting Galaxies at $z=3.1$. *ApJ* **642**, L13–L16.
- GAWISER, E., VAN DOKKUM, P. G., HERRERA, D., MAZA, J., CASTANDER, F. J., INFANTE, L., LIRA, P., QUADRI, R., TONER, R., TREISTER, E., URRY, C. M., ALTMANN, M., ASSEF, R., CHRISTLEIN, D., COPPI, P. S., DURÁN, M. F., FRANX, M., GALAZ, G., HUERTA, L., LIU, C., LÓPEZ, S., MÉNDEZ, R., MOORE, D. C., RUBIO, M., RUIZ, M. T., TOFT, S. & YI, S. K. 2006*b* The Multiwavelength Survey by Yale-Chile (MUSYC): Survey Design and Deep Public UBVRIZ’ Images and Catalogs of the Extended Hubble Deep Field-South. *ApJ* **162**, 1–19.
- GEHRELS, N. 1986 Confidence limits for small numbers of events in astrophysical data. *ApJ* **303**, 336–346.
- GIACCONI, R., ZIRM, A., WANG, J., ROSATI, P., NONINO, M., TOZZI, P., GILLI, R., MAINIERI, V., HASINGER, G., KEWLEY, L., BERGERON, J., BORGANI, S., GILMOZZI, R., GROGIN, N., KOEKEMOER, A., SCHREIER, E., ZHENG, W. & NORMAN, C. 2002 Chandra Deep Field South: The 1 Ms Catalog. *ApJ* **139**, 369–410.
- GIAVALISCO, M. *et al.* 2004 The Great Observatories Origins Deep Survey: Initial Results from Optical and Near-Infrared Imaging. *ApJ* **600**, L93–L98.
- GILLI, R. 2004 The X-ray background and the deep X-ray surveys. *Advances in Space Research* **34**, 2470–2477.

- GILLI, R., COMASTRI, A. & HASINGER, G. 2007 The synthesis of the cosmic X-ray background in the Chandra and XMM-Newton era. *A&A* **463**, 79–96.
- GILLI, R., SALVATI, M. & HASINGER, G. 2001 Testing current synthesis models of the X-ray background. *A&A* **366**, 407–417.
- GRUBER, D. E., MATTESON, J. L., PETERSON, L. E. & JUNG, G. V. 1999 The Spectrum of Diffuse Cosmic Hard X-Rays Measured with HEAO 1. *ApJ* **520**, 124–129.
- HARRISON, F. A., ECKART, M. E., MAO, P. H., HELFAND, D. J. & STERN, D. 2003 The Serendipitous Extragalactic X-Ray Source Identification Program. I. Characteristics of the Hard X-Ray Sample. *ApJ* **596**, 944–956.
- HASINGER, G. 2000 X-ray Surveys of the Obscured Universe. In *ISO Survey of a Dusty Universe* (ed. D. Lemke, M. Stickle & K. Wilke), *Lecture Notes in Physics*, Berlin Springer Verlag, vol. 548, pp. 423–+.
- HASINGER, G., CAPPELLUTI, N., BRUNNER, H., BRUSA, M., COMASTRI, A., ELVIS, M., FINOGUENOV, A., FIORE, F., FRANCESCHINI, A., GILLI, R., GRIFFITHS, R. E., LEHMANN, I., MAINIERI, V., MATT, G., MATUTE, I., MIYAJI, T., MOLENDI, S., PALTANI, S., SANDERS, D. B., SCOVILLE, N., TRESSE, L., URRY, C. M., VETTOLANI, P. & ZAMORANI, G. 2007 The XMM-Newton Wide-Field Survey in the COSMOS Field. I. Survey Description. *ApJ* **172**, 29–37.
- HASINGER, G. *et al.* 2001 XMM-Newton observation of the Lockman Hole. I. The X-ray data. *A&A* **365**, L45–L50.
- HAUSER, M. G. & DWEK, E. 2001 The Cosmic Infrared Background: Measurements and Implications. *ARA&A* **39**, 249–307.
- HICKOX, R. C., JONES, C., FORMAN, W. R., MURRAY, S. S., BRODWIN, M., XBOOTES, T. C., IRAC SHALLOW SURVEY, S., AGES & NOAO DWFS TEAMS 2006 X-ray and infrared properties of galaxies and AGNs in the 9 square degree Bootes field. *ArXiv Astrophysics e-prints*.
- KASHLINSKY, A., MATHER, J. C. & ODENWALD, S. 1996 Clustering of the Diffuse Infrared Light from the COBE DIRBE Maps: an All-Sky Survey of C(0). *ApJ* **473**, L9+.
- KIM, D.-W. *et al.* 2004 Chandra Multiwavelength Project. I. First X-Ray Source Catalog. *ApJ* **150**, 19–41.
- KING, A. 2005 The AGN-Starburst Connection, Galactic Superwinds, and $M_{BH}-\sigma$. *ApJ* **635**, L121–L123.
- LAWRENCE, A. 2001 Quasars, Starbursts, and the Cosmic Energy Budget. In *The Promise of the Herschel Space Observatory* (ed. G. L. Pilbratt, J. Cernicharo, A. M. Heras, T. Prusti & R. Harris), *ESA Special Publication*, vol. 460, pp. 95–+.
- LEHMER, B. D., BRANDT, W. N., ALEXANDER, D. M., BAUER, F. E., SCHNEIDER, D. P., TOZZI, P., BERGERON, J., GARMIRE, G. P., GIACCONI, R., GILLI, R., HASINGER, G., HORNSCHMEIER, A. E., KOEKEMOER, A. M., MAINIERI, V., MIYAJI, T., NONINO, M., ROSATI, P., SILVERMAN, J. D., SZOKOLY, G. & VIGNALI, C. 2005 The Extended Chandra Deep Field-South Survey: Chandra Point-Source Catalogs. *ApJ* **161**, 21–40.
- LILLY, S. J., FÈVRE, O. L., RENZINI, A., ZAMORANI, G., SCODEGGIO, M., CONTINI, T., CAROLLO, C. M., HASINGER, G., KNEIB, J.-P., IOVINO, A., LE BRUN, V., MAIER, C., MAINIERI, V., MIGNOLI, M., SILVERMAN, J., TASCA, L. A. M., BOLZONELLA, M., BONGIORNO, A., BOTTINI, D., CAPAK, P., CAPUTI, K., CIMATTI, A., CUCCIATI, O., DADDI, E., FELDMANN, R., FRANZETTI, P., GARILLI, B., GUZZO, L., ILBERT, O., KAMPCZYK, P., KOVAC, K., LAMAREILLE, F., LEAUTHAUD, A., BORGNE, J.-F. L., MCCracken, H. J., MARINONI, C., PELLO, R., RICCIARDELLI, E., SCARLATA, C., VERGANI, D., SANDERS, D. B., SCHINNERER, E., SCOVILLE, N., TANIGUCHI, Y., ARNOUITS, S., AUSSEL, H., BARDELLI, S., BRUSA, M., CAPPI, A., CILIEGI, P., FINOGUENOV, A., FOUCAUD, S., FRANCESCHINI, R., HALLIDAY, C., IMPEY, C., KNOBEL, C., KOEKEMOER, A., KURK, J., MACCAGNI, D., MADDOX, S., MARANO, B., MARCONI, G., MENEUX, B., MOBASHER, B., MOREAU, C., PEACOCK, J. A., PORCIANI, C., POZZETTI, L., SCARAMELLA, R., SCHIMINOVICH, D., SHOPBELL, P., SMAIL, I., THOMPSON, D., TRESSE, L., VETTOLANI, G., ZANICHELLI, A. & ZUCCA, E. 2007 zCOSMOS: A Large VLT/VIMOS Redshift Survey Covering $0 < z < 3$ in the COSMOS Field. *ApJ* **172**, 70–85.
- LONSDALE, C. J. *et al.* 2003 SWIRE: The SIRTf Wide-Area Infrared Extragalactic Survey. *PASP* **115**, 897–927.

- MAGDZIARZ, P. & ZDZIARSKI, A. A. 1995 Angle-dependent Compton reflection of X-rays and gamma-rays. *MNRAS* **273**, 837–848.
- MAINIERI, V., ROSATI, P., TOZZI, P., BERGERON, J., GILLI, R., HASINGER, G., NONINO, M., LEHMANN, I., ALEXANDER, D. M., IDZI, R., KOEKEMOER, A. M., NORMAN, C., SZOKOLY, G. & ZHENG, W. 2005 The Chandra deep field South/GOODS survey. Optically faint X-ray sources. *A&A* **437**, 805–821.
- MALIZIA, A., BASSANI, L., STEPHEN, J. B., DI COCCO, G., FIORE, F. & DEAN, A. J. 2003 BeppoSAX Average Spectra of Seyfert Galaxies. *ApJ* **589**, L17–L20.
- MARKWARDT, C. B., TUELLER, J., SKINNER, G. K., GEHRELS, N., BARTHELMEY, S. D. & MUSHOTZKY, R. F. 2005 The Swift/BAT High-Latitude Survey: First Results. *ApJ* **633**, L77–L80.
- MATSUMOTO, T., MATSUURA, S., MURAKAMI, H., TANAKA, M., FREUND, M., LIM, M., COHEN, M., KAWADA, M. & NODA, M. 2005 Infrared Telescope in Space Observations of the Near-Infrared Extragalactic Background Light. *ApJ* **626**, 31–43.
- MATT, G., FABIAN, A. C., GUAINAZZI, M., IWASAWA, K., BASSANI, L. & MALAGUTI, G. 2000 The X-ray spectra of Compton-thick Seyfert 2 galaxies as seen by BeppoSAX. *MNRAS* **318**, 173–179.
- MATUTE, I., LA FRANCA, F., POZZI, F., GRUPPIONI, C., LARI, C., ZAMORANI, G., ALEXANDER, D. M., DANESE, L., OLIVER, S., SERJEANT, S. & ROWAN-ROBINSON, M. 2002 The evolution of type 1 active galactic nuclei in the infrared ($15\mu\text{m}$): the view from ELAIS-S1. *MNRAS* **332**, L11–L14.
- MORRISON, R. & MCCAMMON, D. 1983 Interstellar photoelectric absorption cross sections, 0.03–10 keV. *ApJ* **270**, 119–122.
- NENKOVA, M., IVEZIĆ, Ž. & ELITZUR, M. 2002 Dust Emission from Active Galactic Nuclei. *ApJ* **570**, L9–L12.
- PAPOVICH, C., DOLE, H., EGAMI, E., LE FLOC’H, E., PÉREZ-GONZÁLEZ, P. G., ALONSO-HERRERO, A., BAI, L., BEICHMAN, C. A., BLAYLOCK, M., ENGELBRACHT, C. W., GORDON, K. D., HINES, D. C., MISSELT, K. A., MORRISON, J. E., MOULD, J., MUZEROLLE, J., NEUGEBAUER, G., RICHARDS, P. L., RIEKE, G. H., RIEKE, M. J., RIGBY, J. R., SU, K. Y. L. & YOUNG, E. T. 2004 The 24 Micron Source Counts in Deep Spitzer Space Telescope Surveys. *ApJ* **154**, 70–74.
- PEROLA, G. C., MATT, G., CAPPI, M., FIORE, F., GUAINAZZI, M., MARASCHI, L., PETRUCCI, P. O. & PIRO, L. 2002 Compton reflection and iron fluorescence in BeppoSAX observations of Seyfert type 1 galaxies. *A&A* **389**, 802–811.
- QUADRI, R., MARCHESINI, D., VAN DOKKUM, P., GAWISER, E., FRANX, M., LIRA, P., RUDNICK, G., URRY, C. M., MAZA, J., KRIEK, M., BARRIENTOS, L. F., BLANC, G. A., CASTANDER, F. J., CHRISTLEIN, D., COPPI, P. S., HALL, P. B., HERRERA, D., INFANTE, L., TAYLOR, E. N., TREISTER, E. & WILLIS, J. P. 2007 The Multiwavelength Survey by Yale-Chile (MUSYC): Deep Near-Infrared Imaging and the Selection of Distant Galaxies. *AJ* **134**, 1103–1117.
- RISALITI, G., MAIOLINO, R. & SALVATI, M. 1999 The Distribution of Absorbing Column Densities among Seyfert 2 Galaxies. *ApJ* **522**, 157–164.
- ROSATI, P., TOZZI, P., GIACCONI, R., GILLI, R., HASINGER, G., KEWLEY, L., MAINIERI, V., NONINO, M., NORMAN, C., SZOKOLY, G., WANG, J. X., ZIRM, A., BERGERON, J., BORGANI, S., GILMOZZI, R., GROGIN, N., KOEKEMOER, A., SCHREIER, E. & ZHENG, W. 2002 The Chandra Deep Field-South: The 1 Million Second Exposure. *ApJ* **566**, 667–674.
- ROVILOS, E., GEORGAKAKIS, A., GEORGANTOPOULOS, I., AFONSO, J., KOEKEMOER, A. M., MOBASHER, B. & GOUDIS, C. 2007 Radio observations of the Chandra Deep Field South. Exploring the possible link between radio emission and star formation in X-ray selected AGN. *A&A* **466**, 119–126.
- SANDERS, D. B., SALVATO, M., AUSSEL, H., ILBERT, O., SCOVILLE, N., SURACE, J. A., FRAYER, D. T., SHETH, K., HELOU, G., BROOKE, T., BHATTACHARYA, B., YAN, L., KARTALTEPE, J. S., BARNES, J. E., BLAIN, A. W., CALZETTI, D., CAPAK, P., CARILLI, C., CAROLLO, C. M., COMASTRI, A., DADDI, E., ELLIS, R. S., ELVIS, M., FALL, S. M., FRANCESCINI, A., GIAVALISCO, M., HASINGER, G., IMPEY, C., KOEKEMOER, A., LE FÈVRE, O., LILLY, S., LIU, M. C., MCCRACKEN, H. J., MOBASHER, B., RENZINI, A., RICH, M., SCHINNERER, E., SHOPBELL, P. L., TANIGUCHI, Y., THOMPSON, D. J., URRY, C. M. & WILLIAMS, J. P. 2007 S-COSMOS: The Spitzer Legacy Survey of the Hubble

- Space Telescope ACS 2 deg² COSMOS Field I: Survey Strategy and First Analysis. *ApJ* **172**, 86–98.
- SAZONOV, S., REVNIVTSEV, M., KRIVONOS, R., CHURAZOV, E. & SUNYAEV, R. 2007 Hard X-ray luminosity function and absorption distribution of nearby AGN: INTEGRAL all-sky survey. *A&A* **462**, 57–66.
- SCHNEIDER, D. P., HALL, P. B., RICHARDS, G. T., STRAUSS, M. A., VANDEN BERK, D. E., ANDERSON, S. F., BRANDT, W. N., FAN, X., JESTER, S., GRAY, J., GUNN, J. E., SUBBARAO, M. U., THAKAR, A. R., STOUGHTON, C., SZALAY, A. S., YANNY, B., YORK, D. G., BAHCALL, N. A., BARENTINE, J., BLANTON, M. R., BREWINGTON, H., BRINKMANN, J., BRUNNER, R. J., CASTANDER, F. J., CSABAI, I., FRIEMAN, J. A., FUKUGITA, M., HARVANEK, M., HOGG, D. W., IVEZIĆ, Ž., KENT, S. M., KLEINMAN, S. J., KNAPP, G. R., KRON, R. G., KRZESIŃSKI, J., LONG, D. C., LUPTON, R. H., NITTA, A., PIER, J. R., SAXE, D. H., SHEN, Y., SNEDDEN, S. A., WEINBERG, D. H. & WU, J. 2007 The Sloan Digital Sky Survey Quasar Catalog. IV. Fifth Data Release. *AJ* **134**, 102–117.
- SCHNEIDER, D. P. *et al.* 2002 The Sloan Digital Sky Survey Quasar Catalog. I. Early Data Release. *AJ* **123**, 567–577.
- SCOVILLE, N., ABRAHAM, R. G., AUSSEL, H., BARNES, J. E., BENSON, A., BLAIN, A. W., CALZETTI, D., COMASTRI, A., CAPAK, P., CARILLI, C., CARLSTROM, J. E., CAROLLO, C. M., COLBERT, J., DADDI, E., ELLIS, R. S., ELVIS, M., EWALD, S. P., FALL, M., FRANCESCHINI, A., GIAVALISCO, M., GREEN, W., GRIFFITHS, R. E., GUZZO, L., HASINGER, G., IMPEY, C., KNEIB, J.-P., KODA, J., KOEKEMOER, A., LEFEVRE, O., LILLY, S., LIU, C. T., MCCRACKEN, H. J., MASSEY, R., MELLIER, Y., MIYAZAKI, S., MOBASHER, B., MOULD, J., NORMAN, C., REFREGIER, A., RENZINI, A., RHODES, J., RICH, M., SANDERS, D. B., SCHIMINOVICH, D., SCHINNERER, E., SCODEGGIO, M., SHETH, K., SHOBELL, P. L., TANIGUCHI, Y., TYSON, N. D., URRY, C. M., VAN WAERBEKE, L., VETTOLANI, P., WHITE, S. D. M. & YAN, L. 2007a COSMOS: Hubble Space Telescope Observations. *ApJ* **172**, 38–45.
- SCOVILLE, N., AUSSEL, H., BRUSA, M., CAPAK, P., CAROLLO, C. M., ELVIS, M., GIAVALISCO, M., GUZZO, L., HASINGER, G., IMPEY, C., KNEIB, J.-P., LEFEVRE, O., LILLY, S. J., MOBASHER, B., RENZINI, A., RICH, R. M., SANDERS, D. B., SCHINNERER, E., SCHIMINOVICH, D., SHOBELL, P., TANIGUCHI, Y. & TYSON, N. D. 2007b The Cosmic Evolution Survey (COSMOS): Overview. *ApJ* **172**, 1–8.
- SETTI, G. & WOLTJER, L. 1989 Active Galactic Nuclei and the spectrum of the X-ray background. *A&A* **224**, L21–L23.
- SILK, J. & REES, M. J. 1998 Quasars and galaxy formation. *A&A* **331**, L1–L4.
- STANEV, T. & FRANCESCHINI, A. 1998 Constraints on the Extragalactic Infrared Background from Gamma-Ray Observations of MRK 501. *ApJ* **494**, L159+.
- STEFFEN, A. T., STRATEVA, I., BRANDT, W. N., ALEXANDER, D. M., KOEKEMOER, A. M., LEHMER, B. D., SCHNEIDER, D. P. & VIGNALI, C. 2006 The X-ray-to-Optical Properties of Optically-Selected Active Galaxies Over Wide Luminosity and Redshift Ranges. *AJ*, *in press*, astro-ph/0602407.
- TOZZI, P., GILLI, R., MAINIERI, V., NORMAN, C., RISALITI, G., ROSATI, P., BERGERON, J., BORGANI, S., GIACCONI, R., HASINGER, G., NONINO, M., STREBLYANSKA, A., SZOKOLY, G., WANG, J. X. & ZHENG, W. 2006 X-ray spectral properties of active galactic nuclei in the Chandra Deep Field South. *A&A* **451**, 457–474.
- TREISTER, E., CASTANDER, F. J., MACCARONE, T. J., GAWISER, E., COPPI, P. S., URRY, C. M., MAZA, J., HERRERA, D., GONZALEZ, V., MONTOYA, C. & PINEDA, P. 2005 The Calán-Yale Deep Extragalactic Research (CYDER) Survey: Optical Properties and Deep Spectroscopy of Serendipitous X-Ray Sources. *ApJ* **621**, 104–122.
- TREISTER, E. & URRY, C. M. 2005 Active Galactic Nuclei Unification and the X-Ray Background. *ApJ* **630**, 115–121.
- TREISTER, E. & URRY, C. M. 2006 The Evolution of Obscuration in Active Galactic Nuclei. *ApJ* **652**, L79–L82.
- TREISTER, E., URRY, C. M., VAN DUYN, J., DICKINSON, M., CHARY, R.-R., ALEXANDER, D. M., BAUER, F., NATARAJAN, P., LIRA, P. & GROGIN, N. A. 2006 Spitzer Number Counts of AGN in the GOODS fields. *ApJ* **640**, 603–613.
- TREISTER, E. *et al.* 2004 Obscured Active Galactic Nuclei and the X-Ray, Optical, and Far-

- Infrared Number Counts of Active Galactic Nuclei in the GOODS Fields. *ApJ* **616**, 123–135.
- UEDA, Y., AKIYAMA, M., OHTA, K. & MIYAJI, T. 2003 Cosmological Evolution of the Hard X-Ray Active Galactic Nucleus Luminosity Function and the Origin of the Hard X-Ray Background. *ApJ* **598**, 886–908.
- URRY, C. M. & PADOVANI, P. 1995 Unified Schemes for Radio-Loud Active Galactic Nuclei. *PASP* **107**, 803–+.
- VAN DOKKUM, P. G., QUADRI, R., MARCHESINI, D., RUDNICK, G., FRANX, M., GAWISER, E., HERRERA, D., WUYTS, S., LIRA, P., LABBÉ, I., MAZA, J., ILLINGWORTH, G. D., FÖRSTER SCHREIBER, N. M., KRIEK, M., RIX, H.-W., TAYLOR, E. N., TOFT, S., WEBB, T. & YI, S. K. 2006 The Space Density and Colors of Massive Galaxies at $2 < z < 3$: The Predominance of Distant Red Galaxies. *ApJ* **638**, L59–L62.
- VANDEN BERK, D. E. *et al.* 2001 Composite Quasar Spectra from the Sloan Digital Sky Survey. *AJ* **122**, 549–564.
- VIRANI, S. N., TREISTER, E., URRY, C. M. & GAWISER, E. 2006 The Extended Chandra Deep Field-South Survey: X-Ray Point-Source Catalog. *AJ* **131**, 2373–2382.
- WORSLEY, M. A., FABIAN, A. C., BAUER, F. E., ALEXANDER, D. M., HASINGER, G., MATEOS, S., BRUNNER, H., BRANDT, W. N. & SCHNEIDER, D. P. 2005 The unresolved hard X-ray background: the missing source population implied by the Chandra and XMM-Newton deep fields. *MNRAS* **357**, 1281–1287.
- YANG, Y., MUSHOTZKY, R. F., STEFFEN, A. T., BARGER, A. J. & COWIE, L. L. 2004 The Chandra Large Area Synoptic X-Ray Survey (CLASXS) of the Lockman Hole-Northwest: The X-Ray Catalog. *AJ* **128**, 1501–1523.